

# Catastrophic eruption of magnetic flux rope in the corona and solar wind with and without magnetic reconnection

Y. Chen<sup>1,2</sup>, Y. Q. Hu<sup>2</sup>, AND S. J. SUN<sup>2</sup>

## ABSTRACT

It is generally believed that the magnetic free energy accumulated in the corona serves as a main energy source for solar explosions such as coronal mass ejections (CMEs). In the framework of the flux rope catastrophe model for CMEs, the energy may be abruptly released either by an ideal magnetohydrodynamic (MHD) catastrophe, which belongs to a global magnetic topological instability of the system, or by a fast magnetic reconnection across preexisting or rapidly-developing electric current sheets. Both ways of magnetic energy release are thought to be important to CME dynamics. To disentangle their contributions, we construct a flux rope catastrophe model in the corona and solar wind and compare different cases in which we either prohibit or allow magnetic reconnection to take place across rapidly-growing current sheets during the eruption. It is demonstrated that CMEs, even fast ones, can be produced taking the ideal MHD catastrophe as the only process of magnetic energy release. Nevertheless, the eruptive speed can be significantly enhanced after magnetic reconnection sets in. In addition, a smooth transition from slow to fast eruptions is observed when increasing the strength of the background magnetic field, simply because in a stronger field there is more free magnetic energy at the catastrophic point available to be released during an eruption. This suggests that fast and slow CMEs may have an identical driving mechanism.

*Subject headings:* Sun: corona – Sun: magnetic fields – Sun: coronal mass ejections(CMEs)

## 1. INTRODUCTION

It is generally believed that the accumulated magnetic free energy serves as a main energy source for the spectacular solar eruptive phenomena such as coronal mass ejections (CMEs) (see reviews by Forbes (2000) and Low (2001)), but it remains open how the magnetic energy is released. Among various scenarios, the flux rope catastrophe mechanism is a very promising one (reviewed recently by Lin et al. (2003) and Hu (2005)). The catastrophe is an ideal magnetohydrodynamic (MHD) process belonging to a global magnetic topological instability of the system. It releases energy without ohmic heating, especially

suitable for CMEs without associated flares (e.g., Forbes & Isenberg, 1991; Isenberg et al., 1993; Forbes & Priest, 1995; Hu et al., 2003b). A by-product of the catastrophe is the formation of one or more electric current sheets, which grows at the Alfvénic time scale and provides proper sites for fast magnetic reconnection. Such a reconnection further releases the stored magnetic energy and should be responsible for a solar flare associated with a CME event (e.g., Forbes & Lin, 2000; Lin & Forbes, 2000). Thus, in terms of this scenario, there are two means of magnetic energy release process involved in solar eruptions, which are the ideal MHD catastrophe and resistive magnetic reconnection. Both processes are thought to be important to the CME initiation and acceleration. It is therefore necessary and important to disentangle their contributions to the CME dynamics and energetics. This article serves as a first step to solve this problem under the framework of the

<sup>1</sup>Institute for Space Sciences, Shandong University; Department of Space Science and Applied Physics, Shandong University at Weihai, Weihai Shandong, 264209 China; yaochen@sdu.edu.cn

<sup>2</sup>School of Earth and Space Sciences, University of Science and Technology of China, Hefei Anhui 230026, China

specific catastrophe model for CMEs.

The eruptive flux rope after catastrophe is accelerated mainly by the net or unbalanced Lorentz force, which is contributed by various source currents both inside and outside the flux rope, including that along each electric current sheet and the corresponding image current, and the background potential field which is determined by the normal component of the background field at the solar surface. To reveal the roles of these various components of magnetic forces in sustaining the flux rope in equilibrium and causing the eruption, Chen et al. (2006b) conducted detailed force balance analyses. It was found that the primary lifting force is provided by the azimuthal current inside the rope and its image below the photosphere, which is mainly balanced by the pulling force produced by the background potential field when the rope is in equilibrium. During an eruption of the rope caused by the catastrophe, the force associated with the rapidly-developing current sheet(s) constitutes an additional and significant restoring force that decelerates the rope. This force will be greatly reduced or even eliminated once magnetic reconnection sets in across the current sheet(s), as a consequence the magnetic reconnection may cause a further acceleration of the flux rope. This will be confirmed and quantified by the calculations presented in this article with an axisymmetric flux rope catastrophe model. The effect of the solar wind plasma with an equatorial current sheet above the streamer cusp point extending to infinity is considered so as to get a more realistic description of the CME acceleration and propagation. Note that in most previous studies on the flux rope catastrophe this effect was not included. Sun & Hu (2005) did consider the effect of the solar wind on the rope catastrophe and the consequent eruption. They suggested that the flux rope catastrophe can serve as a mechanism for slow CMEs. Yet, they investigated only the cases corresponding to a relatively weak background field in terms of ideal MHD. Based on their work, we take the effect of both the solar wind and magnetic reconnection into account in the present study, which may be regarded as a starting point to disentangle the impacts of MHD catastrophe and magnetic reconnection on the CME dynamics in the solar wind. We put our focus on the differences between the flux rope dynamics in two situations in which

we either prohibit or allow magnetic reconnection to take place across the rapidly-growing current sheets. We introduce the background corona and solar wind model and the flux rope catastrophe model in the following section. In § 3.1 we compare the solutions with and without magnetic reconnection to illustrate its impact on the CME dynamics. We emphasize the effect of the background magnetic field strength in § 3.2 and provide a brief summary of this article with discussions in the last section of this article.

## 2. FLUX ROPE CATASTROPHE MODEL IN THE CORONA AND SOLAR WIND

Coronal magnetic flux ropes are in essence three-dimensional structures with two ends anchored to the photosphere. Considering that the length of a magnetic flux rope is much larger than its diameter, the axisymmetrical simplification (also called 2.5-D models) can be used to approximate the realistic flux rope system. With this approximation, the magnetic field  $\mathbf{B}$  can be expressed with a magnetic flux function  $\psi(t, r, \theta)$  in spherical coordinates  $(r, \theta, \varphi)$ ,

$$\mathbf{B} = \nabla \times \left( \frac{\psi}{r \sin \theta} \hat{\varphi} \right) + B_\varphi \hat{\varphi}. \quad (1)$$

The derived resistive MHD equations in spherical coordinates are written into the following form (see also Ding et al., 2006):

$$\frac{\partial \rho}{\partial t} + \nabla \cdot (\rho \mathbf{v}) = 0, \quad (2)$$

$$\begin{aligned} \frac{\partial \mathbf{v}}{\partial t} + \mathbf{v} \cdot \nabla \mathbf{v} + \frac{1}{\rho} \nabla p + \frac{1}{\mu \rho} [L \psi \nabla \psi + \mathbf{B}_\varphi \times (\nabla \times \mathbf{B}_\varphi)] \\ + \frac{1}{\mu \rho r \sin \theta} \nabla \psi \cdot (\nabla \times \mathbf{B}_\varphi) \hat{\varphi} + \frac{GM_\odot}{r^2} \hat{r} = 0, \end{aligned} \quad (3)$$

$$\frac{\partial \psi}{\partial t} + \mathbf{v} \cdot \nabla \psi - \frac{1}{\mu} \eta r^2 \sin^2 \theta L \psi = 0, \quad (4)$$

$$\begin{aligned} \frac{\partial B_\varphi}{\partial t} + r \sin \theta \nabla \cdot \left( \frac{B_\varphi \mathbf{v}}{r \sin \theta} \right) + [\nabla \psi \times \nabla \left( \frac{v_\varphi}{r \sin \theta} \right)]_\varphi \\ - \frac{1}{r \sin \theta} \nabla \eta \cdot \nabla (\mu r \sin \theta B_\varphi) - \frac{1}{\mu} \eta r \sin \theta L (r B_\varphi \sin \theta) = 0, \end{aligned} \quad (5)$$

$$\frac{\partial T}{\partial t} + \mathbf{v} \cdot \nabla T + (\gamma - 1) T \nabla \cdot \mathbf{v} - \frac{\gamma - 1}{\rho R} \eta j^2 = 0, \quad (6)$$

where

$$L \equiv \frac{1}{r^2 \sin^2 \theta} \left( \frac{\partial^2}{\partial r^2} + \frac{1}{r^2} \frac{\partial^2}{\partial \theta^2} - \frac{\cot \theta}{r^2} \frac{\partial}{\partial \theta} \right), \quad (7)$$

$$\mathbf{j} = \frac{1}{\mu} \nabla \times \mathbf{B} = -\frac{1}{\mu} r \sin \theta L \psi \hat{\varphi} + \frac{1}{\mu} \nabla \times (B_\varphi \hat{\varphi}). \quad (8)$$

The symbols  $\rho$ ,  $\mathbf{v}$ ,  $T$ , and  $\mathbf{j}$  represent the density, flow velocity, temperature and the current density, respectively.  $\mu$  is the vacuum magnetic permeability,  $R$  the gas constant,  $G$  the gravitational constant,  $M_\odot$  the solar mass, and  $\gamma$  the polytropic index which is taken to be 1.05 so as to obtain a reasonable solution of the background steady-state solar wind. The temperature and density at the coronal base are taken to be  $T_0 = 2 \times 10^6$  K and  $\rho_0 = 1.67 \times 10^{-13}$  kg m<sup>-3</sup>, respectively. The magnetic flux function at the coronal base is taken to be the same as a dipolar field given by  $\psi(r = R_\odot) = \psi_0 \sin^2 \theta / R_\odot$  where  $\psi_0 = B_0 R_\odot^2$ .  $B_0$  represents half of the magnetic field strength at the polar hole ( $\theta = 0$ ) on the solar surface, which can be used to represent the strength of the background magnetic field of the system. Note that in this study the magnetic flux function at the solar surface is fixed to its initial distribution which is determined by  $B_0$ . For the effect of the photospheric magnetic flux distribution on the coronal flux rope catastrophe, please check a recent paper written by Sun et al. (2007). The parameter  $B_0$  will be freely adjusted. For example,  $\psi_0 = 9.7 \times 10^{13}$  Wb with  $B_0$  taken to be 2 G giving the case investigated by Sun & Hu (2005). It is defined that the ideal MHD situation corresponds to a zero magnetic resistivity  $\eta$ . In the resistive situation, an anomalous homogeneous resistivity is used with  $\eta$  given by  $\eta = \eta_0 \mu v_{s0} R_\odot$  where  $\eta_0 = 0.1$  and  $v_{s0} = \sqrt{2RT_0} = 181.8$  km s<sup>-1</sup>. The steady-state polytropic solar wind solution is obtained by solving the above MHD equations with  $\eta = 0$ . The magnetic topology (white lines) and the velocity color contour map for  $B_0 = 6$  G from  $1 R_\odot$  to  $20 R_\odot$  are illustrated in Figure 1a. For other values of  $B_0$ , the field topology and velocity distribution are basically similar to that shown in this figure. It can be seen that the solution is characterized by a typical streamer-current sheet-solar wind configuration. The cusp point is located at about  $3 R_\odot$ , and the flow velocity reaches up to 400 km s<sup>-1</sup> at about  $10 R_\odot$  along the equator.

Based on the obtained corona and solar wind solution, we let a flux rope with prescribed mass, toroidal and poloidal magnetic fluxes ( $\Psi_p$  and  $\Psi_\varphi$ ) emerge from the equator at the coronal base. The detailed emerging process has been described pre-

viously by Hu et al. (2003b) and Chen et al. (2006a) and will not be repeated here. Special numerical measures are taken to maintain  $\Psi_p$  and  $\Psi_\varphi$  invariant and equal to their initial given values during the simulation (see Hu et al., 2003b). Figure 1b exemplifies the magnetic configuration and velocity contour map of a flux-rope system with the solar wind, where the border of the original flux rope is depicted with a green circle. It can be seen that the closed field region of the streamer expands apparently with the emergence of the flux rope. Such a swelling of a coronal streamer is often observed with the white-light coronagraphs before CMEs (e.g., Howard et al., 1985). The mass contained by the flux rope per radian in the azimuthal direction is set to be  $\frac{0.5}{2\pi} M_0$  where the unit of mass  $M_0 = \rho_0 R_\odot^3 = 5.643 \times 10^{13}$  kg, the poloidal flux  $\Psi_p$  is taken to be 0.3 in units of  $\psi_0$  while the toroidal flux  $\Psi_\varphi$  is changeable. Thus one may find MHD solutions with different values of  $\Psi_\varphi$  to examine whether a catastrophe occurs, and find out the meta-stable state of the system characterized by  $\Psi_p = 0.3$  and a specific value of  $\Psi_\varphi$  which depends on  $B_0$ . Starting from this state any slight increase of  $\Psi_p$  or  $\Psi_\varphi$  may excite the catastrophe. Therefore, the state is taken as the initial state for our simulation of the flux rope eruption. We choose to increase  $\Psi_p$  from 0.3 to 0.305 at  $t = 0$  so as to trigger the catastrophe. Physically speaking, the increase of the poloidal flux can be achieved by a twist of a long three-dimensional flux rope anchored to the photosphere. Besides the mass, magnetic fluxes of the flux rope, the helicity of the flux rope is also of interest to the study on CMEs. In an axisymmetric system like that investigated in this article, the two-dimensional magnetic helicity can be calculated by the following integral according to Hu et al. (1997),

$$H_T = 2\pi \int \int \psi B_\varphi r dr d\theta, \quad (9)$$

where the factor  $2\pi$  comes from the integral over the azimuthal direction, which should be removed if one wants to evaluate the magnetic helicity per radian in the azimuthal direction.

When the flux rope breaks away from the surface and erupts upwards, a current sheet may develop below the flux rope. It is well known that numerical pseudoreconnection takes place across the current sheet in most numerical simulations,

which causes a false transfer of poloidal flux from the background to the flux rope and results in a topological change. In this work, we take special measure to prohibit such numerical reconnection in order to investigate the flux rope dynamics in the framework of ideal MHD. The magnetic flux function  $\psi$  along the current sheet is invariant, which is known a priori, and any reconnection across the sheet reduces it in the present simulation. We therefore reassign  $\psi$  along the current sheet to the known constant value at each time step. This technique, first proposed by Hu et al. (2003b), effectively eliminates numerical reconnection across the equatorial current sheet. Note that this special measure is not employed in our calculations in terms of resistive MHD with a non-zero  $\eta$ .

The calculations are carried out in a domain of  $R_\odot \leq r \leq 30R_\odot$  and  $0 \leq \theta \leq \pi/2$ , which is discretized into  $150 \times 90$  grid points. The grid spacing increases according to a geometric series of a common ratio 1.024 along the radial direction from 0.02 at the solar surface to 0.71 at the top boundary. And a uniform mesh is adopted in the  $\theta$  direction. The multistep implicit scheme developed by Hu (1989) is used to solve the MHD equations. For the eruptive solutions, the calculations are terminated once the top part of the ejecta reaches the upper boundary.

### 3. Numerical results

In this section, we first present and compare the solutions given by the ideal and resistive MHD calculations for the case with  $B_0 = 6$  G as a first step to disentangle the impacts of MHD catastrophe and magnetic reconnection on the CME dynamics in the solar wind. Then, we investigate the effect of the background magnetic field strength by comparing results with different values of  $B_0$ .

#### 3.1. Impact of magnetic reconnection on flux rope dynamics

As mentioned previously, our simulations on the flux rope catastrophe and eruption start from an equilibrium state which is a meta-stable flux rope system in the corona and solar wind background. The catastrophe is triggered by a slight increase of the poloidal flux  $\Psi_p$  of the flux rope from 0.3 to 0.305 (or  $8.7 - 8.85 \times 10^{13}$  Wb in phys-

ical units) at  $t = 0$  with the critical axial flux in the rope  $\Psi_\varphi = 0.209$  ( $6.06 \times 10^{13}$  Wb) for  $B_0 = 6$  G. After that, the flux rope starts to break away from the photosphere and erupts upwards. Figures 1c and 1d show the magnetic topology and velocity color contours at the same instant ( $t = 280$  minutes) for the two solutions with and without magnetic reconnection (i.e., the cases with  $\eta \neq 0$  and  $\eta = 0$ ). An apparent difference between the two solutions lies in whether a current sheet develops below the flux rope. The sheet forms and grows with the rope eruption in the ideal MHD case, while it is eroded by magnetic reconnection in the resistive MHD calculation. It is also apparent that a significant part of the poloidal flux has been transferred from the background to the flux rope, and a new streamer appears as the aftermath of magnetic reconnection in the resistive calculation. The rate of magnetic flux transfer is mainly determined by the effective resistivity consisting of the anomalous resistivity and the numerical resistivity involved in the pseudoreconnection. Unfortunately, at this time, it is not possible to eliminate the pseudoreconnection in our calculations in terms of resistive MHD. Therefore, it is difficult to control the flux transfer rate by simply adjusting the magnetic resistivity in this case. Further discussion regarding this issue will be given in our discussion section. Another major difference is the color distribution of the velocity contour maps which indicates how fast the flux rope erupts. It can be seen that the rope erupts faster in the solution with magnetic reconnection, as will be quantitatively revealed in Figure 2.

In Figure 2, we plot the profiles of the heliocentric distance, velocity, and acceleration of different parts of the flux rope ejecta, including the cusp point (in dotted), the rope top (in dashed), the rope axis (in solid), and the rope bottom (in dot-dashed), left panels for the case without reconnection and right for the reconnection case. It can be seen that in both cases the flux rope starts to take off at  $t \approx 70$  minutes. There is an apparent delay of about 50 minutes of the time when the cusp point starts to move upwards rapidly. The delay reflects the time taken for the eruptive flux rope to propagate from the coronal base to the initial cusp point location in the corona. We can see that the cusp point undergoes the most dramatic acceleration in both cases: in about 70 minutes the

velocity of the cusp point reaches up to  $800 \text{ km s}^{-1}$  with the maximum acceleration being  $300 \text{ m s}^{-2}$  in the ideal case, and  $1200 \text{ km s}^{-1}$  and  $500 \text{ m s}^{-2}$  for the resistive one. On the other hand, it takes 2 to 3 hours for the flux rope to be accelerated to the maximum speed. After the maximum, the velocities become more or less constant. The velocities of different parts of the ejecta vary significantly from the cusp point to the rope bottom. For example, at  $t = 280$  minutes the exact moment at which the snapshot is taken for Figure 1, the velocity decreases monotonically from about  $800 \text{ km s}^{-1}$  at the cusp point to  $350 \text{ km s}^{-1}$  at the rope bottom in the ideal case, and from  $1100 \text{ km s}^{-1}$  to  $750 \text{ km s}^{-1}$  in the resistive case. This monotonic decrease of velocities from the leading to trailing edges has been often observed by measurements of flux-rope like structures in the interplanetary space (e.g., Gosling et al., 1998), which simply indicates that the rope undergoes a rapid expansion during its eruption. The velocity profiles given by both solutions in Figure 2 as well as that in the following figure are in a good agreement with a recent statistical study on the CME accelerations, which indicates that a CME usually undergoes multiphased kinematic evolution including an initial slow rise phase and a main rapid acceleration phase in the inner corona, and a relatively smooth propagation phase in the outer corona (Zhang & Dere, 2006). The magnitude and duration of the main acceleration given by our calculations are also in line with their statistical results. Taking the resistive case shown in Figure 2 as an example, the main acceleration phase starts from  $t \approx 70$  minutes and ends at about  $t = 190$  minutes lasting for nearly 2 hours. Comparing the solutions with and without magnetic reconnection, it is apparent that the speeds and accelerations of the flux rope are significantly enhanced in the case involved with magnetic reconnection. Further discussions regarding the roles of magnetic reconnection in the CME dynamics will be given in our discussion section.

### 3.2. Effect of background field strength

In this subsection, we present numerical results given by calculations with different values of the parameter  $B_0$ , which represents the strength of the background field and directly relates to the amounts of magnetic energy that can be stored and released in the system. In Figure 3, we plot

radial profiles of the velocity and acceleration of different parts of the system including the cusp point (in dotted), and the rope top (in dashed), axis (in solid), and bottom (in dot-dashed) for the cases with (thick lines) and without (thin lines) reconnection, the left panels are for the solution with  $B_0 = 2 \text{ G}$  and the right panels with  $B_0 = 10 \text{ G}$ . Note that for clearness only the accelerations of the cusp point and rope axis are plotted in the lower panels. Similar to the above calculation the catastrophe is triggered by a slight increase of the dimensionless poloidal flux inside the rope  $\Psi_p$  from 0.3 to 0.305 with the corresponding critical dimensionless axial flux  $\Psi_\varphi$  equal to 0.129 for the case with  $B_0 = 2 \text{ G}$  and 0.244 for  $B_0 = 10 \text{ G}$ . Note that the magnetic fluxes in physical units are listed in Table 1. Since the relative magnitude of the rope poloidal flux does not change with varying  $B_0$ , the size of the flux rope does not change apparently either. To be quantitatively, we checked the heliocentric distance of the rope axis  $r_a$  which can be used to represent the size of the flux rope. It was found that  $r_a = 1.42, 1.52$ , and  $1.54$  solar radii for the cases with  $B_0 = 2, 6$ , and  $10 \text{ G}$ , respectively. As a result, the plasma density inside the flux rope gets slightly different in different cases since the total mass contained by the rope does not change with  $B_0$ . In Table 1, we also list the two-dimensional magnetic helicity per radian in the azimuthal direction  $H_T$  calculated with Equation (9). Similar as the rope fluxes,  $H_T$  also increases dramatically with increasing  $B_0$ . We see that the physical properties of the flux rope differ significantly from case to case in our calculations, which naturally have impacts on the flux rope dynamics. Further discussion along this direction will be presented at the end of the following paragraph.

It can be seen from Figure 3 that the most obvious difference between the two sets of solution is the magnitude of velocity and acceleration at different points of the ejecta. In the resistive calculation with  $B_0 = 2 \text{ G}$ , the main acceleration phase of the flux rope lasts for about 4 hours from  $t \approx 100$  minutes to  $t \approx 350$  minutes with speeds rising up to  $670 \text{ km s}^{-1}$  at the cusp point and to  $460 \text{ km s}^{-1}$  at the rope bottom, which is followed by the so-called propagation phase with a nearly constant speed (Zhang & Dere, 2006). In the ideal calculation with the same value of  $B_0$ , the velocity keeps increasing till  $t = 600$  minutes, yet the

corresponding acceleration gets smaller than  $5 \text{ m s}^{-2}$ . In the resistive case with  $B_0 = 10 \text{ G}$ , the main acceleration phase lasts for about 2 hours starting from  $t \approx 40$  minutes and ending at about  $t = 150$  minutes with the maximum acceleration rising up to  $750 \text{ m s}^{-2}$ . After the maximum of velocity is reached, which is about  $1600 \text{ km s}^{-1}$  for the cusp point and  $1150 \text{ km s}^{-1}$  for the rope bottom, the flux rope gets decelerated gradually to a velocity of  $1300 \text{ km s}^{-1}$  at the cusp point and  $900 \text{ km s}^{-1}$  at the rope bottom. In the ideal case with  $B_0 = 10 \text{ G}$ , the main acceleration phase also lasts for about 2 hours with the maximum acceleration being about  $430 \text{ m s}^{-2}$  for the cusp point and  $220 \text{ m s}^{-2}$  for the rope axis. In the propagation phase following the velocity maximum, the velocities decrease slightly. It can be seen that CMEs, even fast ones, can be produced taking the ideal MHD catastrophe as the only process of magnetic energy release. It is also true, again, that the eruptive speeds are significantly enhanced after magnetic reconnection sets in. We point it out in passing that a smooth transition of eruptions from slow to fast can be obtained when varying  $B_0$  continuously with a stronger background field corresponding to a faster eruption, in line with the very recent study on the effect of photospheric flux distribution on the flux rope dynamics by Sun et al. (2007). The physical cause of such a behavior can be easily understood from the following simple energy analysis. Since the pattern of the magnetic flux distribution at the coronal base remains the same for all cases we have discussed, the associated open field energy must be proportional to the square of  $B_0$ . On the other hand, the percentage by which the catastrophic energy threshold exceeds the open field energy varies in a much smaller range. It reads 6.1%, 8.8% and 9.6% for  $B_0 = 2 \text{ G}$ ,  $6 \text{ G}$  and  $10 \text{ G}$ , respectively. Such a result is consistent with previous similar calculations (e.g., Hu et al., 2003b; Li & Hu, 2003; Chen et al., 2006a). Therefore, the total amount of magnetic free energy of the system at the catastrophic point is mainly determined by the overall strength of the background field in spite of the dramatic differences in the flux rope properties at the catastrophic point as listed in Table 1. In summary, we argue that the stronger the background field is, the more magnetic free energy is available for the flux rope system at the catastrophic point,

which leads to a faster eruption of the flux rope.

To shed more light on the effect of magnetic reconnection on the CME dynamics, we calculate the total increase in kinetic energy of the system compared with that of the pre-eruption state (i.e., the state at  $t = 0$ ), represented by  $\Delta E_k$ . Figure 4 shows the temporal profiles of  $\Delta E_k$  per radian in the azimuthal direction in units of  $5.38 \times 10^{31}$  ergs for the three sets of solutions with  $B_0=2 \text{ G}$  (in solid),  $6 \text{ G}$  (in dotted), and  $10 \text{ G}$  (in dashed), where thick and thin lines represent the results with and without magnetic reconnection. The velocity and acceleration for these solutions have been illustrated in Figures 2 and 3. We can see that  $\Delta E_k$  tends to reach an asymptotic value in all cases. For each set of solutions, the asymptotic value of  $\Delta E_k$  in the resistive case is about 2 to 3 times of that in the ideal case indicating that the MHD catastrophe and magnetic reconnection, the two means of magnetic energy release process, are of comparable importance on the CME acceleration for the resistive MHD situation.

#### 4. Conclusions and discussion

In terms of the catastrophe theory, there are two main processes energizing the solar eruptions: MHD catastrophe and magnetic reconnection. This article serves as a first step to disentangle their contributions to the CME dynamics. To do this, we construct a flux rope catastrophe model in the corona and solar wind and compare different cases in which we either prohibit or allow magnetic reconnection to take place across rapidly-growing current sheets during the eruption. For simplicity, a polytropic process with the polytropic index  $\gamma = 1.05$  is used to produce the background solar wind solution. The catastrophe and the consequent eruption is triggered by a tiny increase of the rope poloidal flux, which reflects a slight twist of the ends of a long three-dimensional realistic flux rope anchored to the photosphere. It is demonstrated that CMEs, even fast ones, can be produced taking the ideal MHD catastrophe as the only process of magnetic energy release. Nevertheless, the eruptive speed can be significantly enhanced after magnetic reconnection sets in. In addition, a smooth transition from slow to fast eruptions is yielded when increasing the strength of the background magnetic field, i.e., a

stronger field, in which more free magnetic energy gets available at the catastrophic point, enables a faster eruption. This suggests that fast and slow CMEs may have an identical driving mechanism.

Based on previous and present studies taking catastrophe as the principle driving mechanism of CMEs, we argue that the MHD catastrophe is probably the main means of energy release for CMEs at least in the initial phase. It releases energy without ohmic heating and provide accelerations with the Lorentz force, especially suitable for non-flare associated CMEs. A by-product of the catastrophe is the formation of one or more electric current sheets, which proceeds at the Alfvénic time scale and produces conditions favoring fast magnetic reconnection. Such a reconnection, if takes place, further releases the magnetic energy through the following two aspects. Firstly, the magnetic energy is converted into thermal and kinetic energies of plasma particles at the reconnection site. This process is believed to account for a solar flare associated with a CME event. Secondly, the restoring force contributed by the current in the current sheet is significantly reduced or even eliminated, and the magnetic topology changes with the magnetic reconnection. This also produces a significant acceleration of the flux rope in addition to that caused by catastrophe. It can be seen from our quantitative calculation that the MHD catastrophe and magnetic reconnection, the two magnetic energy release processes, may have comparable impacts on the CME dynamics during the main acceleration phase of CMEs.

A major subject of this article is to estimate the impact of magnetic reconnection on the flux rope dynamics. For this purpose, we compared solutions given by calculations with and without magnetic reconnection. However, this work suffers from the facts that the anomalous magnetic resistivity is artificially given and the numerical pseudoreconnection is unavoidable in the resistive calculations. Since the effective resistivity including both the anomalous and the numerical ones is believed to be much larger than the realistic value in the corona and solar wind, the velocity profiles given by our study for the case with magnetic reconnection should be taken as the upper bound for the realistic situation. As mentioned in the text, the effective resistivity is a crucial factor determining the transfer rate of magnetic

flux from the background to the flux rope. Observationally, this transfer rate can be evaluated by extrapolating the photospheric field to the corona and counting the change of the total magnetic flux in the aftermath of a CME event, e.g., in the coronal dimming region (see, e.g., Jing et al., 2005 and Qiu & Yurchyshyn, 2005). Further theoretical endeavor should utilize these relevant observational constraints on the flux transfer rate in the modelling of a specific event.

Our study on the effect of magnetic field strength reveals a smooth transition from slow to fast eruptions when increasing the background field strength. This is in support of the argument that slow and fast CMEs may be driven by a single identical mechanism, also in line with recent statistical results contradicting with the traditional bimodal classification of slow (gradual) and fast (impulsive) CMEs (e.g., Sheeley et al., 1999; Andrews & Howard, 2001). For instance, it is shown by Yurchyshyn et al. (2005) and Zhang & Dere (2006) that the velocity and acceleration of a large amount of CME events have a continuous distribution instead of a bimodal one, and by Vršnak et al. (2005) that flare- and nonflare- associated CMEs have quite similar characteristics in the LASCO C2 and C3 fields of view. The velocity profiles for slow CMEs given by our model, say, the solution corresponding to a weak background field, show a gradual acceleration, while that for fast CMEs present a rapid acceleration and a discernable deceleration following the main acceleration phase. This behavior is probably a result of the coupling process with the background solar wind plasma according to our preliminary analysis. When the magnetic energy released in an eruption is not enough to accelerate the flux rope ejecta to the speed of the background plasmas, the ejecta may get gradually accelerated and gain more energy through the coupling to the solar wind. On the other hand, the ejecta may get decelerated and lose energy through similar coupling process with the solar wind while the released magnetic energy is enough to push the flux rope outwards with a velocity faster than that of the background.

There exist contradicting discrepancies between the present thick-rope model in axisymmetrical spherical geometry and that published in the literature in terms of thin-rope models in 2-D cartesian geometry. Firstly, an infinite amount of energy is

required to open up a closed magnetic field in 2-D Cartesian geometry (Hu et al., 2003b), therefore, it is energetically impossible to open the overlying field and to let the flux rope escape to infinity without magnetic reconnection, as demonstrated by the catastrophe models assuming Cartesian geometry (e.g., Lin & Forbes, 2000). On the other hand, in the spherical geometry the corresponding open-field energy is finite and it can be exceeded by the flux rope system as already shown by many calculations (e.g., Choe & Cheng, 2002; Hu et al., 2003b; Li & Hu, 2003; Flyer et al., 2004; Sun & Hu, 2005; Zhang et al., 2005; Peng & Hu, 2005; Ding & Hu, 2006; Chen et al., 2006a). Thus, magnetic reconnection may not be necessarily required for the flux rope to get escaped from the Sun in the spherical model. Secondly, as pointed out previously, the self-interaction of the azimuthal current inside the flux rope by itself results in an outward radial force on the rope, which comes from the curvature of the rope surrounding the Sun (Chen, 1989; Lin et al., 1998; Krall et al., 2000; Chen et al., 2006b). This self-force, together with that contributed by its image current below the photosphere, serves as a dominant driving force for the rope eruption. However, in the 2-D Cartesian models this self-force is trivially zero by the symmetry of an infinitely long straight current, this gives another basic difference between the 2-D Cartesian and spherical models.

No matter what geometry is used, so far most flux rope models have been limited to 2-D analyses, as a necessary simplification for practical tractability. Yet, the two ends of a 3-D flux rope are believed to be anchored to the solar surface. It remains open regarding how the catastrophic behavior of the flux rope may change under this situation. Finally, since how the corona and solar wind plasma is heated and accelerated is still a big issue to be resolved, the polytropic process is assumed conveniently to obtain the reasonable background solar wind solution in this work. However, it should be noted that the polytropic solar wind solution is too simple to account for some realistic properties of the solar wind. For example, the effect of the fast solar wind is not included in this study. This will certainly affect the propagation of the ejecta at high latitudes, yet may not be very important to the study on the CME propagation along the equatorial plane. In future we

consider to employ sophisticated heating functions to produce a more realistic solar wind background (see, e.g., Chen & Hu, 2001; Hu et al., 2003a) for a more elaborated study on the CME propagation in the meridional plane.

This work was supported by grants NNSFC 40404013, NSBRSP G2006CB806304, and NNSFC 10233050 in China.

## REFERENCES

Andrews, M. D., & Howard, R. S. 2001, *Space Sci. Rev.*, 95, 147

Chen, J., 1989, *ApJ*, 338, 453

Chen, Y., Chen, X. H., & Hu, Y. Q. 2006a, *ApJ*, 644, 587

Chen, Y., & Hu, Y. Q. 2001, *Sol. Phys.*, 199, 371

Chen, Y., Li, G. Q., & Hu, Y. Q. 2006b, *ApJ*, 649, 1093

Choe, G. S., & Cheng C. Z., 2002, *ApJ*, 574, L179

Ding, J. Y., & Hu, Y. Q., 2006, *Sol. Phys.*, 199, 371

Ding, J. Y., Hu, Y. Q., & Wang, J. X., 2006, *Sol. Phys.*, 235, 223

Flyer, N., Fornberg, B., Thomas, S., & Low, B. C., 2004, *ApJ*, 606, 1210

Forbes, T. G., 2000, *J. Geophys. Res.*, 105, 23153

Forbes, T. G., & Isenberg, P. A., 1991, *ApJ*, 373, 294

Forbes, T. G., & Lin, J., 2000, *J. Atmos. Sol.-Terr. Phys.*, 62, 1499

Forbes, T. G., & Priest, E. R., 1995, *ApJ*, 446, 377

Gosling, J. T., Riley, P., McComas, D. J., & Pizzo, V. J., 1998, *J. Geophys. Res.*, 103, 1941

Howard, R. A., Sheely, N. R., Jr., Koomen, M. J., & Michels, D. J. 1985, *J. Geophys. Res.*, 90, 8173

Hu, Y. Q. 1989, *J. Comput. Phys.*, 84, 441

Hu, Y. Q. 2005, in IAU Symp. 266, Coronal and Stellar Mass Ejections, ed. K. Dere, J. Wang, & Y. Yan (Cambridge: Cambridge Univ. press), 263

Hu, Y. Q., Habbal, S. R., Chen, Y., & Li, X., 2003a, 108(A10), 1377, doi:10.1029/2002JA009776

Hu, Y. Q., Li, G. Q., & Xing X. Y. 2003b, J. Geophys. Res., 108(A2), 1072, doi:10.1029/2002JA009419

Hu Y. Q., Xia L. D., Li X, Wang J. X., & Ai G. X., 1997, Sol. Phys., 170, 283

Isenberg, P. A., Forbes, T. G., & Demoulin, P., 1993, ApJ, 417, 368

Jing, J., Qiu, J., Lin, J., Qu, M., Xu, Y., & Wang, H., 2005, ApJ, 620, 1085

Krall, J., Chen, J., & Santoro, R., 2000, ApJ, 539, 964

Li, G. Q., & Hu, Y. Q. 2003, Chinese J. Astron. Astrophys., 3, 555

Lin, J., & Forbes, T. G. 2000, J. Geophys. Res., 105(A2), 2375

Lin, J. Forbes, T. G., Isenberg, P. A., & Demoulin, P., 1998, ApJ, 504, 1006

Lin, J., Soon, W., & Baliunas, S. L. 2003, NewA Rev., 47, 53

Low, B. C., 2001, J. Geophys. Res., 106, 25141

Peng, ZH., & Hu, Y. Q. 2005, Chinese J. Space Sci., 25, 81

Qiu, J., & Yurchyshyn, V. B., 2005, ApJ, 634, L121

Sheeley, N. R., Jr., Walters, H., Wang, Y.-M., & Howard, R. A. 1999, J. Geophys. Res., 104, 24739

Sun, S. J., & Hu, Y. Q. 2005, J. Geophys. Res., 110, A05102, doi:10.1029/2004JA010905

Sun, S. J., Hu, Y. Q., & Chen, Y., 2007, ApJ, 654, L167

Vršnak, B., Sudar, D., & Ruzdjak, D. 2005, A&A, 435, 1149

Yurchyshyn, V., Yashiro, S., Abramenko, V., Wang, H., & Gopalswamy, N. 2005, ApJ, 619, 599

Zhang, J., & Dere, K. P. 2006, ApJ, 649, 1100

Zhang, Y. Z., Hu, Y. Q., & Wang, J. X. 2005, ApJ, 626, 1096

Table 1. The poloidal and toroidal fluxes ( $\Psi_{pc}$  and  $\Psi_{\varphi c}$ ), and the two-dimensional magnetic helicity  $H_T$  (per radian in the azimuthal direction) of the flux rope system at the catastrophic point in different cases.

| $B_0$ (G)                | 2                     | 6                     | 10                    |
|--------------------------|-----------------------|-----------------------|-----------------------|
| $\Psi_{pc}$ (Wb)         | $2.91 \times 10^{13}$ | $8.70 \times 10^{13}$ | $1.45 \times 10^{14}$ |
| $\Psi_{\varphi c}$ (Wb)  | $1.25 \times 10^{13}$ | $6.06 \times 10^{13}$ | $1.08 \times 10^{14}$ |
| $H_T$ (Wb <sup>2</sup> ) | $1.45 \times 10^{27}$ | $2.12 \times 10^{28}$ | $6.32 \times 10^{28}$ |

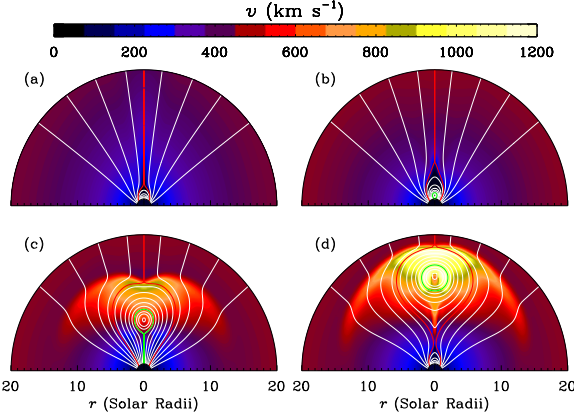


Fig. 1.— The magnetic topology (white lines) and velocity color contour map for  $B_0 = 6$  G from  $1 R_\odot$  to  $20 R_\odot$  for: (a) the background corona and solar wind solution before the emergence of the flux rope, (b) the pre-eruption state of the flux-rope system in the solar wind background, (c) the solution with an erupting flux rope at  $t = 280$  minutes without magnetic reconnection, and (d) the eruptive solution with magnetic reconnection at the same instant as panel (c). The outer boundary of the original flux rope is depicted with a green circle.

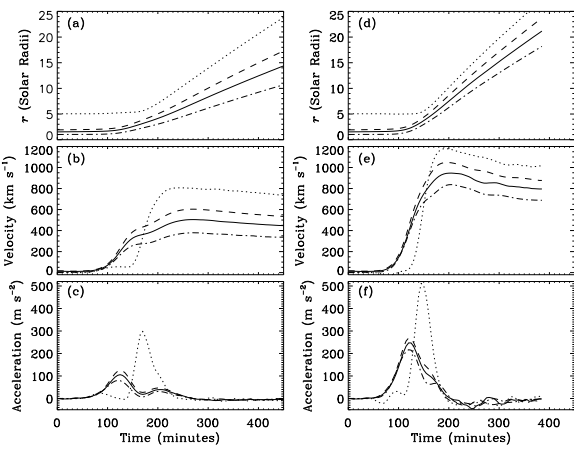


Fig. 2.— The temporal profiles of the heliocentric distance, velocity, and acceleration of different parts of the flux rope system, including the cusp point (in dotted), the rope top (in dashed), the rope axis (in solid), and the rope bottom (in dot-dashed). Left panels are for the case without reconnection and right for the reconnection case.

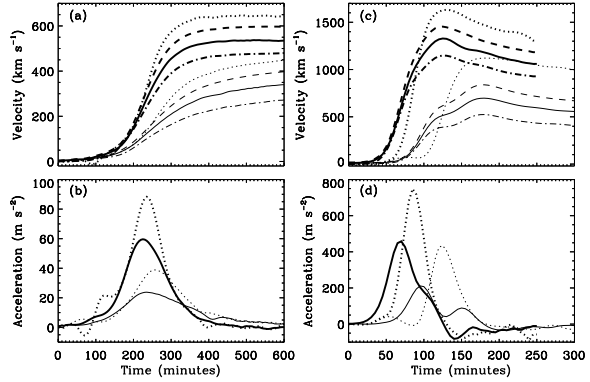


Fig. 3.— The radial profiles of the velocity and acceleration of different parts of the system including the cusp point (in dotted), and the rope top (in dashed), axis (in solid), and bottom (in dot-dashed), the left panels are for the case with  $B_0 = 2$  G and the right panels with  $B_0 = 10$  G for the cases with (thick lines) and without (thin lines) reconnection.

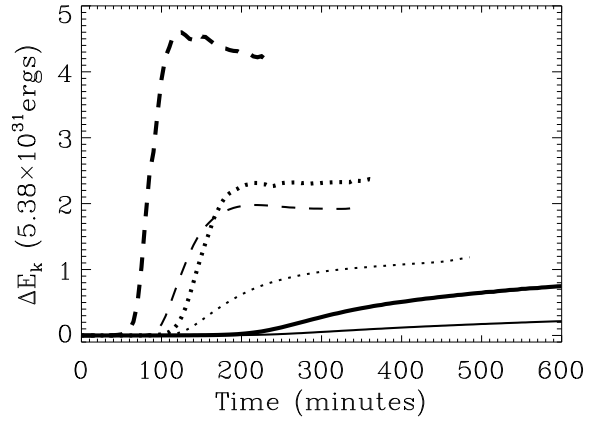


Fig. 4.— The temporal profiles of the total increase in kinetic energy of the system  $\Delta E_k$  in units of  $5.38 \times 10^{31}$  ergs (per radian in the azimuthal direction) for three sets of solutions ( $B_0 = 2$  G (in solid),  $6$  G (in dotted), and  $10$  G (in dashed)) with (thick lines) and without (thin lines) magnetic reconnection.